Cerebral Cortex October 2013;23:2309–2321
doi:10.1093/cercor/bhs220
Advance Access publication August 9, 2012

Functional Connection Between Posterior Superior Temporal Gyrus and Ventrolateral Prefrontal Cortex in Human

P.C. Garell[1], H. Bakken[2], J.D.W. Greenlee[3], I. Volkov[3], R.A. Reale[3], H. Oya[3], H. Kawasaki[3], M.A. Howard[3] and J.F. Brugge[3]

[1]Department of Neurosurgery, New York Medical College, Valhalla, NY, USA [2]Department of Surgery, Madigan Army Medical Center, Fort Lewis, Tacoma, WA 98431, USA [3]Department of Neurosurgery, University of Iowa, Iowa City, IA 52242, USA

Address correspondence to John F. Brugge, Department of Psychology, Brogden Hall, University of Wisconsin, 1202 West Johnson Street, Madison, WI 53706, USA. Email: brugge.johnf@gmail.com

The connection between auditory fields of the temporal lobe and prefrontal cortex has been well characterized in nonhuman primates. Little is known of temporofrontal connectivity in humans, however, due largely to the fact that invasive experimental approaches used so successfully to trace anatomical pathways in laboratory animals cannot be used in humans. Instead, we used a functional tract-tracing method in 12 neurosurgical patients with multicontact electrode arrays chronically implanted over the left ($n = 7$) or right ($n = 5$) perisylvian temporal auditory cortex (area PLST) and the ventrolateral prefrontal cortex (VLPFC) of the inferior frontal gyrus (IFG) for diagnosis and treatment of medically intractable epilepsy. Area PLST was identified by the distribution of average auditory-evoked potentials obtained in response to simple and complex sounds. The same sounds evoked little if there is any activity in VLPFC. A single bipolar electrical pulse (0.2 ms, charge-balanced) applied between contacts within physiologically identified PLST resulted in polyphasic evoked potentials clustered in VLPFC, with greatest activation being in pars triangularis of the IFG. The average peak latency of the earliest negative deflection of the evoked potential on VLPFC was 13.48 ms (range: 9.0–18.5 ms), providing evidence for a rapidly conducting pathway between area PLST and VLPFC.

Keywords: auditory evoked potential, electrical stimulation, functional connectivity

Introduction

The current working model of auditory processing at the forebrain level in humans is based, in large part, on the results of modern anatomical and physiological studies in the monkey (Kaas and Hackett 2005; Hackett 2011). The model envisions multiple auditory cortical fields of the superior temporal gyrus (STG) reciprocally interconnected and arranged in three levels—core, belt, and parabelt—each having its unique connections with the medial geniculate body and related auditory thalamic nuclei. An extension of this model includes anatomically and functionally segregated pathways arising from belt and parabelt areas and reaching auditory-related ventrolateral (VLPFC) and dorsolateral (DLPFC) prefrontal cortices (Hackett et al. 1999; Romanski et al. 1999a, 1999b). Acoustically activated areas of prefrontal cortex are referred to as being "auditory related", as they receive auditory input indirectly by way of "classic" auditory cortex of the temporal lobe and perhaps as well through thalamic, midbrain, limbic, and cerebellar structures which themselves receive sensory input (Fuster 2008). Although many questions of the homology of auditory and auditory-related cortical fields between human and nonhuman primates remain unsettled (Petrides and Pandya 1999, 2002; Hackett et al. 2001; Hackett 2003, 2007, 2008; Sweet et al. 2005; Fullerton and Pandya 2007), the model derived from monkey studies and briefly outlined above serves as an attractive starting point in understanding the structural and functional organizations of auditory cortical processing in the human (Rauschecker and Scott 2009; Kelly et al. 2010). In this paper, we investigate the functional connectivity between auditory cortex on the posterolateral surface of the STG and VLPFC.

Evidence from intracranial electrophysiological (Celesia, 1976; Creutzfeldt and Ojemann 1989; Creutzfeldt et al. 1989a, 1989b; Howard et al. 2000; Crone et al. 2001; Brugge et al. 2003; Edwards et al. 2005, 2009; Bidet-Caulet et al. 2007; Reale et al. 2007; Besle et al. 2008; Steinschneider et al. 2011) and functional imaging (Binder et al. 2000; Hall et al. 2002; Scott and Johnsrude 2003; Hart et al. 2004; Uppenkamp et al. 2006; Voisin et al. 2006) studies in humans have shown that speech and nonspeech sounds activate much of the STG, including the area we refer to as the posterolateral superior temporal (PLST) auditory field (Howard et al. 2000). Cytoarchitectonically, area PLST occupies portions of area 22 of Brodmann (1909), of TA of von Economo (1929), and of Tpt, PaAlt, and TS3 of Galaburda and Sanides (1980). Multiple areas on the superior temporal plane have been identified histochemically along with an area on the lateral surface of STG that appears to overlap PLST (Rivier and Clarke, 1997; Wallace et al. 2002; Chiry et al. 2003). Response properties of PLST distinguish it from those of putative auditory core and adjacent belt cortex on Heschl's gyrus (HG) (Howard et al. 2000) with which it makes functional connections (Brugge et al. 2003, 2005). Whether PLST in humans should be considered the homolog of belt or parabelt cortex in monkey is not clear (Hackett et al. 2001; Hackett 2003, 2007; Sweet et al. 2005; Fullerton and Pandya 2007).

Prefrontal cortex reaches its highest level of development in humans where it occupies that area of the frontal lobe immediately rostral to motor and premotor cortex. It is nonuniform in its cytoarchitecture with multiple fields identified on the lateral surface alone (Petrides and Pandya 1999, 2002). Early direct intracranial recording revealed relatively widespread and overlapping auditory, visual, and somatosensory input to prefrontal cortex (Walter 1964). Subsequent anatomical, physiological, and imaging studies in human and nonhuman primates provide evidence that prefrontal cortex is organized into functional domains that integrate multiple sensory inputs and engage in a number of complex sensorimotor and cognitive processes (Toga and Maziotta, 2000; Stuss and Knight 2002; Romanski 2004; Fuster 2008).

In monkey, DLPFC has been shown to receive auditory cortico-cortical input via a dorsal pathway originating in caudal belt cortex (Pandya and Yeterian 1996; Romanski et al. 1999a, 1999b) although VLPFC appears to receive afferents over this route as well (Petrides and Pandya 2009). Neurons in the acoustic domain of DLPFC are typically, though not exclusively, activated most strongly by sounds arising from particular locations in space (Azuma and Suzuki 1984; Vaadia et al. 1986; Vaadia, 1989), a characteristic that is observed in posterior belt cortical neurons as well (Recanzone 2000). Accordingly, it has been postulated that this temporofrontal circuit is a pathway that conveys primarily spatial information about the sound source. Neurons within a highly restricted region of VLPFC have been shown to respond robustly to a wide range of acoustic signals, including monkey vocalization and human speech (Romanski and Goldman-Rakic 2002; Cohen et al. 2004; Romanski et al. 2005; Russ et al. 2008; Romanski and Averbeck 2009). This acoustic domain of VLPFC in monkey is within the projection field of the anterolateral belt area on the STG (Romanski et al. 1999a, 1999b), which itself contains neurons that are most sensitive to these same complex sounds (Rauschecker et al. 1995; Rauschecker, 1997, 1998; Tian et al. 2001; Rauschecker and Tian 2004). VLPFC is interpreted to be part of a functional stream engaged mainly in identifying complex acoustic signals or "acoustic objects". Information about the "where" and "what" of complex sound is thus postulated to reach prefrontal cortex over dual pathways (Kaas and Hackett, 1999; Rauschecker and Tian, 2000; Scott 2005; Hackett, 2011). While such an arrangement is consistent with indirect findings from functional imaging studies in humans as well (Arnott et al. 2004), there is little direct neurophysiological evidence of these purported functional connections.

Modern neuronal tracer and microelectrode mapping methodologies, which have been so effectively exploited to reveal robust, topographically organized connections between the STG and VLPFC in the nonhuman primate (Petrides and Pandya 1988, 2009; Pandya and Yeterian 1996; Hackett et al. 1999; Romanski et al. 1999a, 1999b) cannot be effectively used in humans. Anatomical magnetic resonance imaging (MRI), diffusion tensor imaging (DTI), and resting state functional connectivity (RSFC) analyses have shown promise in tracing the trajectory of some of the major white matter tracts connecting temporal and frontal lobes (Kier et al. 2004a, 2004b; Catani et al. 2005; Parker et al. 2005; Powell et al. 2006; Glasser and Rilling, 2008; Rilling et al. 2008; Catani 2009; Kelly et al. 2010). Indeed, until the advent of DTI and RSFC, no anatomical tracing of temporofrontal connections in the human brain was carried out save by blunt dissection in autopsy specimens or by microscopic examination of serial tissue sections stained for myelinated axons (e.g. Dejerine 1895; Rosett, 1933). Although DTI provides information on the trajectories of associational white matter tracts, they do little to illuminate the origin, terminal distribution, or transmission properties of these pathways, and RSFC may not exhibit a one-to-one relationship with anatomical connectivity.

We have adopted an alternative method of mapping neural pathways in human cerebral cortex, in neurosurgical patients. The basic approach involves electrical stimulation of one cortical site while recording neural activity evoked by that stimulus from more distant cortical loci (see also Wilson et al. 1990; Liegeois-Chauvel et al. 1991; Matsumoto et al. 2004, 2007). Although this approach provides no direct information on the anatomical trajectories of neural pathways, it does provide information, in the living human brain, on the functional connectivity between the locus of electrical stimulation and the area(s) from which electrically evoked responses are recorded. Using this approach, we have described the functional connections between human core cortex on HG and area PLST (Howard et al. 2000; Brugge et al. 2003, 2005). We also identified functional connectivity within VLPFC (Greenlee et al. 2007) and between VLPFC and orofacial motor cortex (Greenlee et al. 2004). Here we extend these findings, presenting direct electrophysiological evidence for a rapidly conducting pathway that links auditory area PLST with VLPFC in humans.

Materials and Methods

Studies reported here involved recording from, and electrically stimulating, cerebral cortex directly in, 12 adult neurosurgery patients undergoing treatment for medically intractable epilepsy. Results were obtained from multicontact subdural recording arrays placed over the lateral frontal and perisylvian cortices of the left ($n = 7$) or right ($n = 5$) cerebral hemisphere. Age, gender, handedness, and results of sodium amytal (Wada) testing are shown in Table 1. Pure-tone audiograms and speech discrimination scores obtained preoperatively all fell within the normal range. Many of the details of electrode design and implantation as well as electrophysiological recording and electrical stimulation methods have been reported previously (Howard et al. 1996, 2000; Brugge et al. 2003; Greenlee et al. 2004, 2007; Reddy et al. 2010). The experiments were undertaken in accordance with the Declaration of Helsinki. The University of Iowa Institutional Review Committee approved all experimental protocols, and written informed consent was obtained from each subject.

Two multicontact recording grid arrays (Radionics, Burlington, MA, USA) were placed directly on the pial surface in each of the 12 subjects. Clinical considerations dictated the dimensions and placement locations of the arrays. Grid arrays consisted of 8×8 ($n = 5$), 6×10 ($n = 4$), 6×12 ($n = 1$), 5×12 ($n = 1$), or 5×8 ($n = 1$) contacts. Each recording contact was 1.6 mm in diameter with a 5 mm (on center) intercontact separation. One recording array was positioned over the posterolateral aspect of the STG, typically extending onto the perisylvian parietal cortex dorsally and the middle temporal gyrus ventrally. Grids placed over the perisylvian region were most often centered over cortex caudal to the intersection of the central sulcus (CS) and lateral (Sylvian) fissure (LF). These left portions of the middle and anterior STG were unstudied as was the most posterolateral STG that fell beyond reach of most grid placements. The second recording grid array was centered over the IFG, covering much of

Table 1
Age, gender (male/female), handedness (left, right, bilateral, undetermined) and Wada results (left dominant/right dominant/bidominant/not performed) for each of the subjects in the study.

Subject	Age	Gender	Hand	Wada
R21	33	F	R	L
L37	50	M	R	L
L40	48	M	R	L
R42*	39	M	R	L
R43	32	F	R	L
R57*	48	M	L	L
L59	39	F	R	NP
L62	30	F	U	L
L64	53	F	U	R
L66	29	F	R	B
R74*	46	M	R	L
L93*	23	M	R	L

Handedness self-reported in nine subjects and determined using the Geschwind–Oldfield Questionnaire in 1 (L93). Asterisks refer to those subjects whose evoked potential maps, waveforms, and waveform latency measurements are shown in Figures 1–6.

pars triangularis, with limited coverage of pars orbitalis, pars opercularis, and/or other lateral precentral frontal cortices. The placement of these two arrays allowed us to focus on the functional relationship between previously identified temporal auditory field PLST and pars triangularis of the IFG.

In addition to these two grid arrays, four-contact strip electrodes with a 1-cm intercontact spacing were placed on the ventral surface of the inferior temporal gyrus bilaterally. A modified depth electrode (Howard et al. 1996) was also stereotactically implanted roughly parallel to the long axis of HG. Evidence for a functional connection between HG and PLST has been presented previously (Howard et al. 2000; Brugge et al. 2003, 2005).

Intraoperative photographs, post-implantation CT scans, and pre- and postimplantation MRIs were used together in localizing the grid and depth electrode recording sites. A quasi-3D reconstruction was performed on the brain of each patient based on preoperative thin, contiguous MR images using Brainvox (Damasio and Frank 1992; Frank et al. 1997).

Subjects were studied for periods up to 2 weeks while they were undergoing clinical video and electroencephalographic monitoring. Research recordings were usually begun 2 or 3 days after recovery from the implantation surgery. During recording sessions, the subject was usually sitting up awake in the hospital bed or on a nearby recliner. Electrodes remained in place for periods ranging from 7 to 14 days (median: 10 days).

A wide range of acoustic stimuli, including click trains, tone and noise bursts, and consonant vowel (CV) utterances, were presented monaurally or binaurally through insert earphones (Etymotic Research, Elk Grove Village, IL, USA). Earphones were built into an earmold of the kind typically worn by hearing-aid users. Sound stimuli were delivered at a suprathreshold level that was comfortable for each patient (typically 50 dB above the detection threshold). In 10 of the 12 subjects studied, cortical activity was recorded simultaneously from 12 contacts on the surface grid array. Signals were amplified (Bak Electronics, Germantown, MD, USA), filtered (2–500 Hz), and digitized (DataWave, Longmont, CO, USA). Another set of 12 contacts was then chosen for simultaneous recording, and the operation repeated until all contacts on the grid array were sampled and the map completed. In two subjects, studied later in this series, signals were recorded simultaneously from 64 sites on an 8 × 8 grid array, amplified (Grass P15 Preamplifiers, Westbank Warwick, RI, USA), filtered (1–1000 Hz), and digitized (Hewlett Packard VX-1, Palo Alto, CA, USA). Sampling rate was 2, 4, 8, or 10 kHz. With both data acquisition systems, data were stored for off-line analysis using software

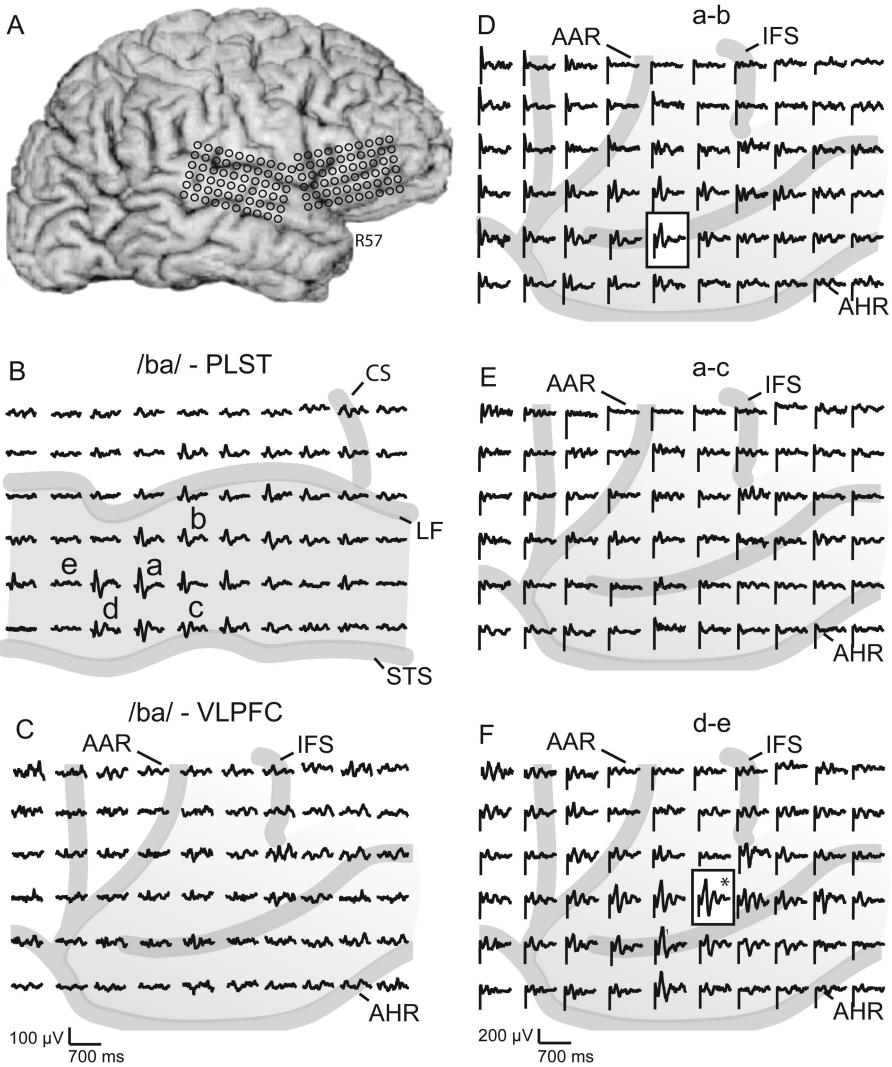

Figure 1. (*A*) Lateral surface-rendered MR image showing locations of recording grids and response fields on STG and VLPFC of right cerebral hemisphere. (*B*) Response fields on posterolateral STG to binaural CV (/ba/) stimulation identify area PLST. Bipolar electrical stimulation of sites within PLST are identified by lower case letters a–d. (*C*) Response field on VLPF to the same /ba/ stimulus. (*D–F*) Response fields on VLPFC to electrical stimulation of three sites (a–b, a–c, d–e) on PLST. CS, central sulcus; LF, lateral fissure; STS, superior temporal sulcus; AAR, anterior ascending ramus of the LF; AHR, anterior horizontal ramus of the LF; PT, pars triangularis. STG and PT identified by shading. Box surrounds site(s) on VLPFC of maximal responsiveness to electrical stimulation of PLST. Asterisk identifies the evoked potential shown expanded in time in Figure 6.

developed under Matlab (Mathworks, Natick, MA, USA). Averaged auditory evoked potentials (AEPs) were computed from 30 to 100 stimulus trials. Negativity is plotted upward in all figures. In all but two subjects, the data acquisition system used computed and saved only the average waveform, discarding individual trials. Hence we did not study evoked gamma-band activity, which may well have been present along with evoked activity represented by the AEP (see Steinschneider et al. 2011).

Once electrophysiological mapping to acoustic stimulation was completed, we initiated electrical-stimulation tract-tracing experiments. A single brief (0.2 ms) charge-balanced electrical pulse was applied in bipolar fashion through a Grass SD9 (constant voltage) or Grass SD12 (constant current) stimulator to adjacent cortical sites within and around functionally identified area PLST while recording from cortex beneath the surface grid on the frontal lobe using the same recording methods described above. The local activation patterns created by this bipolar stimulus configuration can be complex (see Brown et al. 1973; Ranck 1975; Yeomans 1990) but using it proved necessary to minimize the stimulus artifact. Current strengths were maintained below after-discharge threshold (Ojemann and Engel 1986). Electrical stimuli were delivered at a rate of 1 or 2 Hz. The averaged waveform was computed from 30 to 100 stimulus trials and displayed on-line, as described above for acoustic stimulation. Subjects reported no sensations resulting from cortical electrical stimulation with these parameters. Time constraints prevented us from obtaining frontal lobe response maps to

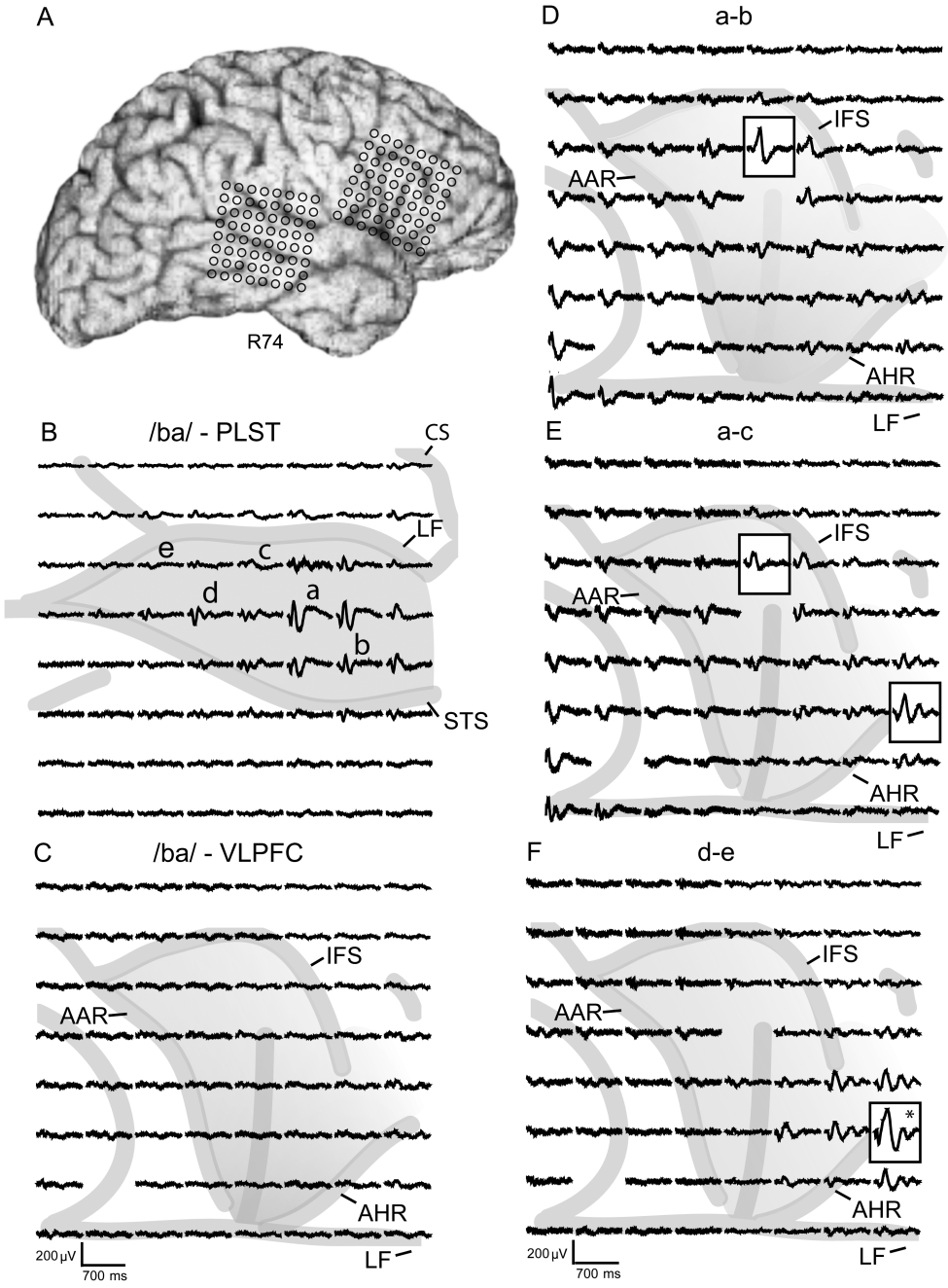

Figure 2. (*A*) Lateral surface-rendered MR image showing locations of recording grids and response fields on STG and VLPFC of right cerebral hemisphere. (*B*) Response fields on posterolateral STG to binaural CV (/ba/) stimulation identify area PLST. Bipolar electrical stimulation of sites within PLST are identified by lower case letters a–d. (*C*) Response field on VLPF to the same /ba/ stimulus. (*D–F*) Response fields on VLPFC to electrical stimulation of three sites (a–b, a–c, d–e) on PLST. See legend of Figure 1 for further details.

electrical stimulation of all of the contacts on lateral STG. Maps to stimulation of two or more STG sites were obtained in 9 of 12 subjects.

In addition to registering the electrophysiological data with MR images of individual subjects, we derived a summary map showing sites of maximal responsiveness in VLPFC to bipolar stimulation of sites in PLST for all 12 subjects. In obtaining this map, intersubject variability in gross anatomical landmarks of the STG and IFG was taken into account by employing a nonlinear elastic transformation method used successfully in our laboratory in mapping deep structures of the human brain (Oya et al. 2009). This approach preserves the spatial relationships between recording and stimulation sites and the surface anatomical features within each subject and then transfers these spatial relationships onto a high-resolution single-subject template image, rendered in Montreal Neurological Institute (MNI) space, provided by the International Consortium for Brain Mapping (ICBM). Individual subject MR images were first aligned with the ICBM template by applying affine (linear) transformations and maximizing normalized mutual information. We then applied a nonlinear thin-plate-smoothing spline algorithm to coregister affine-transformed individual brains to the template brain using eight local anatomical landmarks. Specific stimulation and recording sites identified on both cerebral hemispheres in all subjects were finally mapped onto the single (left) template brain. For our purposes, using local anatomical landmarks to render the image and superimpose stimulation and recording sites in MNI space was more appropriate than carrying out a similar template mapping operation in Talairach space using distant subcortical reference points.

Results

Figures 1–4 are derived from four subjects in whom we were able to stimulate at least three STG sites. In these

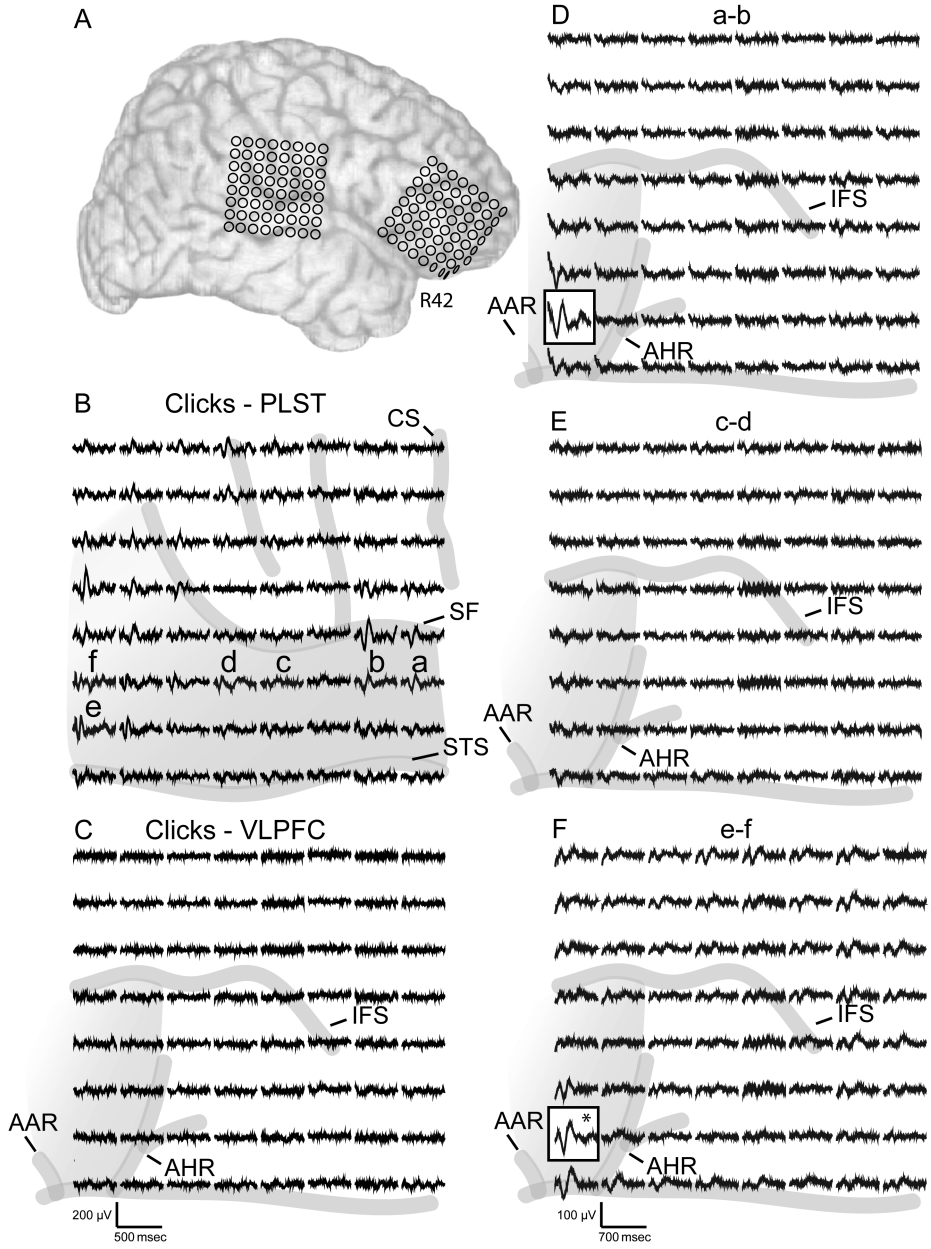

Figure 3. (*A*) Lateral surface-rendered MR image showing locations of recording grids and response fields on STG and VLPFC of right cerebral hemisphere. (*B*) Response fields on posterolateral STG to binaural click-train stimulation identify area PLST. Bipolar electrical stimulation of sites within PLST are identified by lower case letters a–f. (*C*) Response field on VLPF to the same click-train stimulus. (*D–F*) Response fields on VLPFC to electrical stimulation of three sites (a–b, c–d, e–f) on PLST. See legend of Figure 1 for further details.

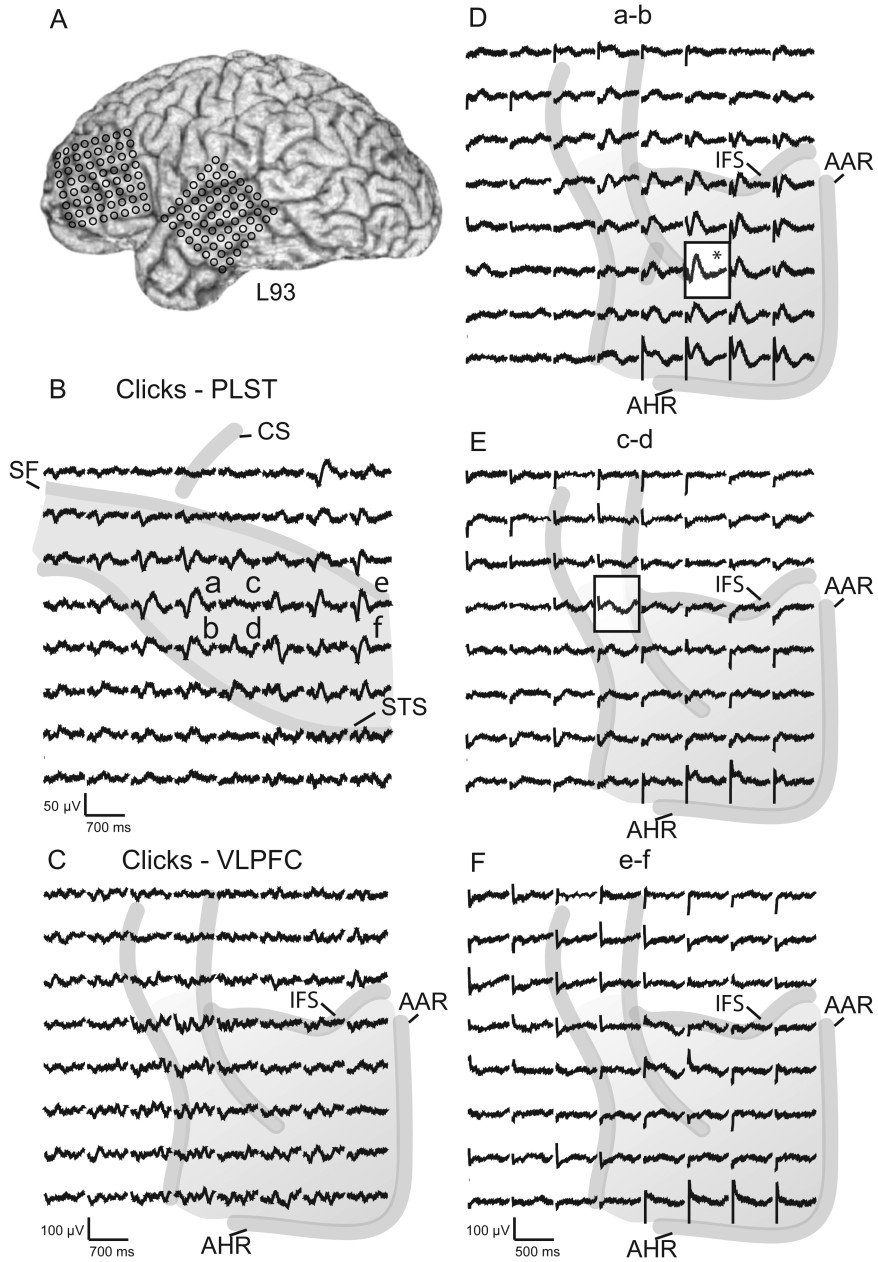

Figure 4. (*A*) Lateral surface-rendered MR image showing locations of recording grids and response fields on STG and VLPFC of a left cerebral hemisphere. (*B*) Response fields on posterolateral STG to binaural click-train stimulation identify area PLST. Bipolar electrical stimulation of sites within PLST are identified by lower case letters a–f. (*C*) Response field on VLPF to the same click-train stimulus. (*D–F*) Response fields on VLPFC to electrical stimulation of three sites (a–b, c–d, e–f) on PLST. See legend of Figure 1 for further details.

figures, the lateral surface-rendered MR images show multicontact grid arrays over frontal and temporal cortices and the waveforms and distributions of averaged evoked potentials recorded from temporal and frontal grids in response to acoustical stimulation and from frontal grids to electrical stimulation of the STG. Whereas the maps and the waveforms from which they were derived varied in detail across subjects, they also exhibited several features common to all subjects in the study. Figure 5 is a map summarizing the spatial pattern of connectivity across subjects, whereas Figure 6 and Table 2 illustrate and summarize data related to the temporal structure of the electrically evoked waveform recorded on VLPFC.

Response of PLST and VLPFC to Acoustical Stimulation

Robust, polyphasic AEPs were recorded over posterolateral STG of both the right (Figs 1B, 2B, and 3B) and left (Fig. 4B) cerebral hemispheres to a wide range of acoustic stimuli, from simple click trains to CV utterances (see also Howard et al. 2000; Brugge et al. 2003; Reale et al. 2007; Steinschneider et al. 2011). AEPs were not uniformly distributed over this region, however. As a rule, a relatively large AEP was seen flanked by AEPs of gradually diminishing amplitude. Commonly, a second cluster of AEPs of lower amplitude and different waveform morphology could be seen separated from the main AEP cluster by relatively unresponsive cortical sites. We refer to this entire area as PLST even though it may be

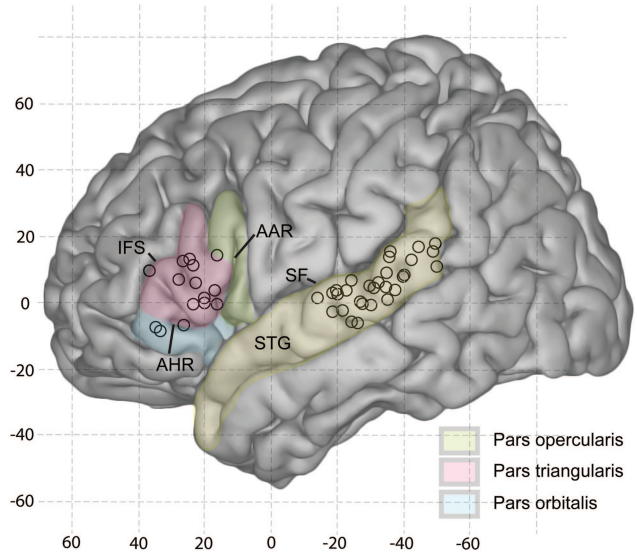

Figure 5. Distribution of sites of maximal amplitude of the response on the IFG to electrical stimulation of sites on posterolateral STG for all subjects in the study. Stimulus and response loci are shown on a template of the left cerebral hemisphere in MNI coordinate space. See Materials and Methods for details.

considered physiologically a mosaic representing perhaps more than one functional auditory field (Howard et al. 2000). Prefrontal cortical sites studied exhibited relatively weak (if any) AEPs in response to the same acoustic stimuli that evoked robust AEPs on PLST (Figs 1C, 2C, 3C, and 4C).

VLPFC Response to PLST Electrical Stimulation

For each of Figures 1–4 are shown three evoked potential maps of VLPFC (D–F) that resulted from electrically stimulating physiologically identified PLST cortex with three different bipolar electrode configurations. Lower case letters above each VLPFC map refer to stimulation sites, which are similarly identified on the acoustical maps of PLST (B) and in the following text. In all cases studied, sites within PLST were identified, which when stimulated electrically evoked robust, polyphasic, time-locked activity in VLPFC. The locus of maximal amplitude of the electrically evoked potential often was flanked by evoked potentials of gradually diminishing amplitude. Stimulation of other sites in PLST yielded little or no evoked activity in VLPFC.

Figure 1B illustrates for one subject the response map obtained from posterolateral STG to the speech utterance /ba/. The waveform and distribution of robust AEPs are characteristic of area PLST, as described above. By comparison, the VLPFC map exhibited widespread low-amplitude oscillations but little sign of AEPs in response to the same acoustic stimulus (Fig. 1C). Electrical stimulation applied across PLST sites a–b, which were most strongly activated by the acoustic stimulus, resulted in robust, polyphasic evoked potentials centered over and essentially confined to pars triangularis (Fig. 1D, rectangle), that prefrontal cortical region (shaded) bounded by the anterior ascending (AAR) and anterior horizontal (AHR) rami of the LF and the IFS. When the stimulus was applied across similarly active PLST sites a–c, however, the resultant map of VLPFC (Fig. 1E) showed little sign of the evoked activity that was obtained when stimulus site a was paired with stimulus site b. Stimulating PLST sites d–e, where the

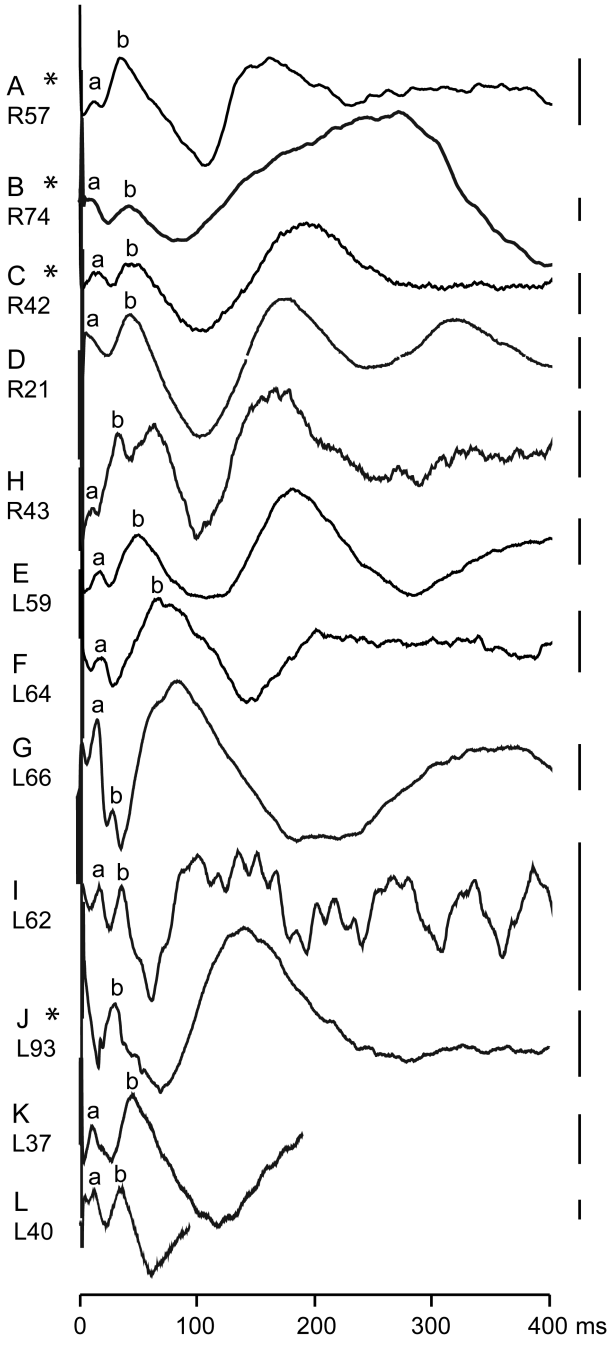

Figure 6. Averaged evoked potentials recorded from the site of maximal responsiveness in VLPFC to electrical stimulation of PLST in each of our 12 subjects (*A–J*). Lower case letters a and b designate peaks of two major negative deflections identified by visual inspection. Latency for each peak with respect to the application of the electrical pulse is given in Table 2. Stimulus artifact appears as a brief voltage pulse at the time of stimulation. Asterisks by evoked potentials identify the sites on the maps shown in Figures 1–4 from which they were derived. Vertical scale to right of each waveform: 50 μV. Filter: B & J: 1–1000 Hz, others: 2–500 Hz.

AEPs were hardly in evidence at all, resulted in evoked activity over pars triangularis (Fig. 1F) that was of demonstrably greater amplitude than that obtained by electrical stimulation of the most acoustically active PLST sites a–b. In other words, activity evoked electrically in this area of VLPFC was not dependent on the stimulus site on PLST being located where strong AEPs were obtained. Two additional

Table 2
Latency to first two negative deflections (a and b) of averaged evoked potential at site of maximal responsiveness in VLPFC to electrical stimulation of the site in PLST giving rise to that evoked potential

Subject	a	b
R57*	13.0	36.4
R74*	14.0	49.5
R42*	14.0	53.4
R21	9.0	36.0
R43	9.0	35.9
L59	17.0	49.4
L64	18.5	67.4
L66	17.2	30.2
L62	14.5	33.4
L37	10.0	47.0
L40	12.1	28.5
L93*	–	27.1
Mean	13.48	41.18
STD	3.28	12.15

Asterisks refer those evoked potentials similarly identified on the maps of Figures 1–4 and the expanded waveforms shown in Figure 6.

observations of note are (1) that a relatively small change in the site of stimulation, from a–b to d–e, resulted in a small shift of the site of maximal responsiveness on VLPFC and (2) evoked potentials clearly extended to cortex caudal to AAR, on pars orbitalis. These shifts in position of the sites of maximal amplitude in VLPFC suggest that the functional projections from the two PLST sites, as shown by maps of Figure 1D and F, while closely overlapping need not be coextensive.

The shift in locus of maximal responsiveness in VLPFC with a change in stimulus site in PLST is seen more clearly in Figure 2, from another subject. The PLST activity time-locked to the utterance /ba/ formed a map similar to the one shown in Figure 1A obtained using the same acoustic stimulus. A high-amplitude AEP was flanked by AEPs of diminishing amplitude. A second focus of activity appeared just caudal to this AEP cluster and was separated from it by a relatively nonresponsive site. The area of VLPFC studied was essentially unresponsive to this utterance. Electrical stimulation of acoustically active sites a–b on PLST evoked a large response on pars triangularis just ventral to the IFS. This site of maximal responsiveness was surrounded by evoked potentials of considerably smaller amplitude and different waveform that were distributed over the remainder of pars triangularis and extending to VLPFC caudal to AAR (pars opercularis) and ventral to AHR (Fig. 2D, pars orbitalis). Figure 2E shows that when electrical stimulation was shifted to PLST sites a–c, two foci of maximal evoked activity appeared on the VLPFC map: one occupied the same site shown in Figure 2D for stimulation of PLST sites a–b, although its amplitude was demonstrably lower, while a larger response appeared on the border between pars triangularis and pars orbitalis. When the electrical pulse was applied across the more caudal sites d–e, which now included the second focus of AEPs within PLST, the evoked potential on the VLPFC map, which was so prominent when more rostral PLST sites were stimulated, was no longer in evidence, whereas the evoked potentials that arose on or near the border of pars triangularis and pars orbitalis became even more prominent (Fig. 2F). Judging from the grid array, we estimate that in the case shown in Figure 2, a shift in the PLST location of 1–2 cm resulted in a shift in the location of maximal activity in pars triangularis of about 2–3 cm.

A quite different projection pattern is illustrated in Figure 3. Here stimulating with click trains (100 Hz, 160 ms duration) resulted in responses depicted in the map of PLST shown in Figure 3B. One cluster of AEPs was located just rostral to the projection of the CS, with the focus of maximal activity located on the lip of the LF. A second focus is identified some 3–4 cm caudally, at the edge of the recording grid. Electrical stimulation across the more rostral sites a–b, located just below the loci of maximal activity, resulted in robust evoked activity very near the AAR, within pars triangularis (Fig. 3D). Again, there was little sign of AEPs on VLPFC or on prefrontal cortex considerably dorsal to the IFS (Fig. 3C). Stimulation across the acoustically activated caudal PLST sites e–f (Fig. 3F) resulted in a robust evoked response at the same recording sites identified in Figure 3D on or just caudal to the AHR. Stimulating sites c–d, between these two active areas of PLST, yielded little in the way of evoked activity in this area of pars triangularis and essentially none over the rest of the VLPFC covered by the recording grid (Fig. 3E).

On the left cerebral hemisphere, click-train stimulation also results in robust AEP activity on posterolateral STG (Fig. 4). Characteristic of PLST, two clusters of AEPs were identified separated by less responsive sites having different waveforms (Fig. 4B). Relatively low-amplitude AEPs were discernible across the area of VLPFC covered by the recording array (Fig. 4C). Stimulation across active PLST sites a–b resulted in a site of maximal responsiveness surrounded by robust evoked potentials of smaller amplitude distributed widely within pars triangularis (Fig. 4D). Stimulation of adjacent and relatively inactive PLST sites c–d yielded only low-amplitude evoked activity on VLPFC (Fig. 4E). Likewise, stimulation across sites e–f, which exhibited strong AEPs in PLST to the click train, resulted in very weak VLPFC responses (Fig. 4F).

Figure 5 presents a summary map of the sites of maximal responsiveness in VLPFC to bipolar stimulation of sites in PLST for all 12 subjects in our study. The sites are projected onto a common high-resolution single-subject template MR image, as described in the Materials and Methods. With a few exceptions, these sites fell within pars triangularis.

Time Waveform and Latency Measurements

Averaged evoked potentials in VLPFC resulting from electrical stimulation of PLST had waveforms characterized by a series of prominent negative deflections occurring within about 300–400 ms after the electrical stimulus was delivered. Shown in Figure 6A–L are AEPs obtained at the site of maximal responsiveness on VLPFC maps of all 12 subjects. Those represented in the evoked potential maps of Figures 1–4 are so indicated by an asterisk (Fig. 6A–C and J). Although there was variability in the waveform across subjects, within about 70 ms after electrical stimulation two major negative deflections were identified in 11 of our 12 subjects (labeled a and b in Fig. 6). Because of interference from the stimulus artifact, the earliest deflection recorded (Fig. 6B and D) was barely discernible, and in one subject (Fig. 6J) was not seen at all. A second deflection (b) was observed in all cases, and its latency varied considerably. Later and broader deflections were also recorded, and in one case (Fig. 6I) the AEP exhibited relatively long lasting oscillations.

Table 2 gives the latency to the peak of each of the earliest identified negative deflection for each subject. The latency to the peak of the earliest (a) deflection ranged from 9.0 to 18.5 ms (mean: 13.48, S.D.: 3.28). We interpret this deflection as the sign of the initial invasion of afferent input to VLPFC resulting from stimulation of PLST. The amplitude and latency of the later deflection (b) exhibited considerably more intersubject variability (mean: 41.19, S.D.: 12.15), with the a-to-b interval ranging from 13.0 to 48.9 ms. This second deflection reflects later arriving afferent activity and/or manifestations of local intracortical processing.

Discussion

The area we mapped acoustically on the posterolateral aspect of the STG corresponds to auditory area PLST, as described previously (Howard et al. 2000; Reale et al. 2007; Steinschneider et al. 2011). In response to a wide range of simple and complex sound, robust polyphasic AEPs were recorded, occasionally at two separate sites, and characterized by a site (or sites) of maximal responsiveness flanked by AEPs of gradually diminishing amplitude. The same acoustic stimuli that activated PLST, including human speech utterances, were relatively ineffective in generating AEPs on VLPFC, although the same VLPFC sites were shown to receive a robust functional projection from PLST.

Although not the primary aim of this study, our finding of a relative lack of responsiveness within human VLPFC cortex to acoustic stimulation seems at odds with results of single neuron recordings from areas 45 and 12vl/47 in monkey. These fields, which together constitute the auditory domain of VLPFC, contain neurons that exhibit robust activity in response to a wide variety of sounds (Romanski and Goldman-Rakic 2002; Cohen et al. 2004; Romanski et al. 2005; Russ et al. 2008; Romanski and Averbeck 2009). Because our electrode grids tended to be centered over pars triangularis (area 45), we were unable to map systematically pars orbitalis, which in human is identified cytoarchitectonically as area 47. Moreover, our stimulation sites were in the posterior aspect of the STG, a region of the monkey STG that would tend to project most heavily on area 12vl/47 (Romanski et al. 1999a, 1999b). It is possible that although areas 45 and 12vl/47 represent in the monkey the acoustic domain of VLPFC, the acoustic domain in the human may be more restricted and hence may have been beyond the reach of our recording arrays (Fecteau et al. 2005). It is unlikely that our auditory stimuli *per se* were not sufficient to evoke responses, as we employed a variety of sounds from click trains to human utterances. Perhaps, activation of VLPFC requires the use of even more complex speech stimuli, for example, speech sounds with emotional overtones (Fecteau et al. 2005). We relied on the AEP to capture mainly the cortical synaptic activity tightly phase locked to the acoustic or electrical stimulus. The AEP does not reveal, however, nonphase-locked activity that might be present in VLPFC recordings as found in PLST recordings, particularly at high gamma band frequencies (Steinschneider et al. 2011). Another possible explanation relates to the level of arousal or attention of our subjects (see Walter 1964). In our experiments, subjects were not required to perform auditory-related tasks but were simply asked to listen to the auditory stimuli. Single-unit studies of the auditory domains of monkey prefrontal cortex cited above show that auditory sensitivity and selectivity of neuronal responses were influenced by task-related behavior. Thus, the fact that we were largely unable to excite pars triangularis and surrounding VLPFC acoustically with stimuli that were highly effective in activating PLST may be attributed not so much to the nature of the sensory stimulus *per se* but to the fact that behavioral conditions were simply not sufficiently favorable to functionally gate the flow of sound evoked activity from PLST to VLPFC target sites.

Typically, in response to bipolar electrical stimulation of adjacent sites in PLST, the resultant evoked potentials recorded on VLPFC were clustered on pars triangularis. This finding of a functional projection from PLST to VLPFC agrees with results obtained in monkey using modern anatomical tract-tracing approaches (Pandya and Yeterian 1996; Hackett et al. 1999; Romanski et al. 1999a, 1999b; Petrides and Pandya 2009) and in humans using RSFC analysis (Kelly et al. 2010). Taking into account some degree of intersubject variability, pars triangularis is generally accepted to be that portion of the IFG occupied by Brodmann's area 45 (Amunts et al. 1999). In the rhesus monkey, cortices of the belt and parabelt systems of the STG project upon prefrontal fields (Hackett et al. 1999; Romanski et al. 1999a, 1999b) including areas exhibiting cytoarchitectonic characteristics similar to those of areas 45 and 47 of human (Petrides and Pandya 2002, 2009).

Time constraints precluded our stimulating all-electrode contacts positioned in PLST. Nonetheless, the response maps obtained showed that changing the stimulating sites within PLST often resulted in demonstrable changes in the size and distribution of evoked activity within pars triangularis. For instance, the robust evoked activity associated with one stimulus configuration could disappear entirely and a new focus of activity associated with the new stimulus configuration could appear. In one instance, however, electrical stimulation of widely separated STG sites of acoustic responsiveness resulted in maximal evoked activity at the same site on the IFG. We also noted that there was not a strong relationship between the magnitude of the auditory evoked response recorded at a PLST site and the magnitude of the evoked potential recorded on VLPFC when electrical stimuli were delivered to that PLST site. Stimulation of some acoustically activated PLST sites could result in no demonstrable evoked activity on VLPFC covered by the recording array. These findings are consistent with modeling data showing that stimulation with adjacent bipolar electrodes is very effective in producing highly localized current flows (Nathan et al. 1993). Taken together, the results suggest that the PLST to VLPFC projection is modular, highly focused, and possibly topographically organized.

The waveform of the electrically evoked potential recorded at the site of maximal responsiveness on VLPFC typically exhibited 2–3 major negative deflections during the first 300–400 ms after an effective electrical stimulus was applied to PLST (in one subject, the stimulus artifact obscured the possible presence of the earliest deflection). The average latency of the peak of the first deflection was 13.48 ms, with onset time occurring several ms earlier. Although somewhat obscured by the stimulus artifact, a deflection as early as 9.0 ms after PLST stimulation was detected in two subjects. The second deflection had peak times ranging from 27.1 to 67.4 ms (mean: 41.18). Using electrical-stimulation tract tracing in human neurosurgical patients, Matsumoto et al. (2004) reported a relatively weak functional projection from the

posterior language area of the temporal lobe to the anterior language area of the frontal lobe. In that report, the functionally connected cortical areas were identified not by their anatomical location or by their responsiveness to acoustic stimulation but by results of clinical (speech arrest) electrical-stimulation functional-mapping methods. In one of their documented cases, electrical stimulation of posterior STG resulted in an averaged evoked potential recorded from a site on VLPFC. Two negative deflections were apparent in the averaged evoked potential, and these had latency values in the range corresponding to the later deflections we describe in the current report. The fact that Matsumoto et al. did not detect earlier evoked activity may have been due to a large electrical artifact associated with the electrical stimulus.

We interpret the earliest deflection we detected in the electrically evoked response as the sign of the initial invasion of afferent input to VLPFC resulting from stimulation of PLST. This evoked activity may have resulted from signal propagation along one or more temporofrontal pathways, as described in monkey (Petrides and Pandya 1988, 2009) and more recently in humans using DTI and anatomical MRI (Kier et al. 2004a, 2004b; Catani et al. 2005; Catani 2009; Glasser and Rilling, 2008; Powell et al. 2006; Parker et al. 2005). One pathway, the arcuate fasciculus, arises from caudal STG (posterior PaAlt and Tpt of Galaburda and Sanides (1980)) and follows a general dorsal and dorso-lateral trajectory around peri-Sylvian cortical regions. The arcuate fasciculus in human has been shown by DTI to be demonstrably larger than the dorsolateral temporofrontal white matter pathway found in the brains of chimpanzees and macaque monkeys (Rilling et al. 2008). A second pathway, which originates in the midregion of STG (PaAlt and TS3 of Galaburda and Sanides (1980)), courses through the external capsule to terminate in VLPFC (including area 45), as well as DLPFC and frontal polar regions. Both caudal and mid-STG sources of temporofrontal projections would likely include neurons within area PLST. The third pathway arises from rostral STG (TS1 and TS2 of Galaburda and Sanides (1980)) and reaches orbitofrontal cortex by way of the uncinate fasciculus. Cortex of STG giving rise to this path is likely rostral to area PLST as mapped in the present experiments.

Taking the arcuate fasciculus to be the longest candidate pathway between PLST and VLPFC, we estimate it to be about 14 cm in length based on MRI measurements. Given this distance and an average *peak* latency of 13.5 ms, the conduction velocity of a subpopulation of axons in this pathway would be 10 m/s, which is well within the limits of conduction velocity of central axons (Waxman and Swadlow 1977). If we take the *onset* latency of the AEP to be considerably shorter than that, then transmission velocity of axons in the arcuate fasciculus could approach 40–50 m/s. If the temporofrontal route of the external capsule were involved, our estimate of the conduction time would be reduced to account for the shorter temporofrontal distance, assuming no intervening synapses. Regardless of the route over which VLPFC was activated by PLST stimulation, the early afferent input could well have arisen from the large (and presumably rapidly conducting) pyramidal cells that populate layers III and V of cortex of the posterolateral STG (Bailey and Bonin 1951; Braak 1978). Although the latency data suggest rapid transmission between PLST and VLPFC, a question remains as to whether this is a monosynaptic relationship. The later deflections in the electrically evoked response are more difficult to interpret. They may represent the invasion of delayed afferent activity arriving over slower conducting or polysynaptic temporofrontal pathways or perhaps local intracortical activity triggered by the earlier afferent volleys. While there are still many unsettled questions regarding the role of the thalamus and other subcortical centers in corticocortical interactions (see Sherman and Guillery 2006), we need also to consider corticothalamic pathways in the context of the functional connectivity observed between a "sensory" cortex on temporal lobe and what has been described as an "action cortex" of prefrontal cortex (Fuster 2008).

The evidence we have provided for a functional connection between an auditory field on posterolateral STG and the IFG applies to both the left and right cerebral hemispheres regardless of handedness and cerebral dominance of the subjects. Considering the possibility that this connectivity is involved in speech/language processing, it would not be surprising to find interhemispheric differences. Whatever those differences may have been, our sample size was too small and/or the intersubject variability was too great to reveal them.

It is now well recognized that seizure activity arising from the mesial temporal lobe can alter neural structures some distance from the seizure focus (Moran et al. 2001; Bernasconi et al. 2004; Thivard et al. 2005; Gross et al. 2006; Mueller et al. 2006; Powell et al. 2007; Focke et al. 2008). While our patient-subjects were diagnosed with medically refractory epilepsy, any pathological changes that might have been associated with their disorder were not of sufficient magnitude to alter the fundamental finding of robust functional connectivity between posterolateral STG and the IFG.

Funding

This work was supported by National Institutes of Health [grant numbers R01DC04290 and M01RR59 (General Clinical Research Centers Program)], the Hoover Fund, and the Carver Trust.

Notes

We thank Daniel Noh for engineering support and Carol Dizack and Tom Weinzerl for graphic artwork. *Conflict of Interest*: None declared.

References

Amunts K, Schleicher A, Burgel U, Mohlberg H, Uylings HBM, Zilles K. 1999. Broca's region revisited: cytoarchitecture and intersubject variability. J Comp Neurol. 412:319–341.

Arnott SR, Binns MA, Grady CL, Alain C. 2004. Assessing the auditory dual-pathway model in humans. Neuroimage. 22:401–408.

Azuma M, Suzuki H. 1984. Properties and distribution of auditory neurons in the dorsolateral prefrontal cortex of the alert monkey. Brain Res. 298:343–346.

Bailey P, Bonin G. 1951. The isocortex of man. Urbana, IL: University of Illinois Press.

Bernasconi N, Duchesne S, Janke A, Lerch J, Collins DL, Bernasconi A. 2004. Whole-brain voxel-based statistical analysis of gray matter and white matter in temporal lobe epilepsy. Neuroimage. 23:717–723.

Besle J, Fischer C, Bidet-Caulet A, Lecaignard F, Bertrand O, Giard MH. 2008. Visual activation and audiovisual interactions in the

auditory cortex during speech perception: intracranial recordings in humans. J Neurosci. 28:14301–14310.
Bidet-Caulet A, Fischer C, Besle J, Aguera PE, Giard MH, Bertrand O. 2007. Effects of selective attention on the electrophysiological representation of concurrent sounds in the human auditory cortex. J Neurosci. 27:9252–9261.
Binder JR, Frost JA, Hammeke TA, Bellgowan PS, Springer JA, Kaufman JN, Possing ET. 2000. Human temporal lobe activation by speech and nonspeech sounds. Cereb Cortex. 10:512–528.
Braak H. 1978. On magnopyramidal temporal fields in the human brain—probable morphological counter parts of Wernicke's sensory speech region. Anat Embryol (Berl). 152:141–169.
Brodmann K. 1909. Vergleichende loakalisationslehre der grosshirnrinde. Leipzig: J.A. Barth.
Brown PB, Smithline L, Halpern B. 1973. Stimulation techniques. In: Brown PB, Maxfield BW, Moraff H, editors. Electronics for neurobiologists. Cambridge, MA: MIT Press.
Brugge JF, Volkov IO, Garell PC, Reale RA, Howard MA. 2003. Functional connections between auditory cortex on Heschl's gyrus and on the lateral superior temporal gyrus in humans. J Neurophysiol. 90:3750–3763.
Brugge JF, Volkov IO, Reale RA, Garell PC, Kawasaki H, Oya H, Li Q, Howard MA. 2005. The posterolateral superior temporal auditory field in humans: functional organization and connectivity. In: Konig R, Heil P, Budinger E, Scheich H, editors. Auditory cortex—toward a synthesis of human and animal research. Mahwah, NJ: Erlbaum. p. 145–162.
Catani M. 2009. Connectional anatomy of language: recent contributions from diffusion tensor tractography. In: Johansen-Berg H, Beherens TEJ, editors. Diffusion MRI: from quantitative measurement to in-vivo neuroanatomy. Amsterdam, the Netherlands: Elsevier. p. 404–412.
Catani M, Jones DK, Dominic H. 2005. Perisylvian language networks of the human brain. Ann Neurol. 57:8–16.
Celesia GG. 1976. Organization of auditory cortical areas in man. Brain. 99:403–414.
Chiry O, Tardif E, Magistretti PJ, Clarke S. 2003. Patterns of calcium-binding proteins support parallel and hierarchical organization of human auditory areas. Eur J Neurosci. 17:397–410.
Cohen YE, Russ BE, Gifford GW, III, Kiringoda R, MacLean KA. 2004. Selectivity for the spatial and nonspatial attributes of auditory stimuli in the ventrolateral prefrontal cortex. J Neurosci. 24:11307–11316.
Creutzfeldt O, Ojemann G. 1989. Neuronal activity in the human lateral temporal lobe. III. Activity changes during music. Exp Brain Res. 77:490–498.
Creutzfeldt O, Ojemann G, Lettich E. 1989a. Neuronal activity in the human lateral temporal lobe. I. Responses to speech. Exp Brain Res. 77:451–475.
Creutzfeldt O, Ojemann G, Lettich E. 1989b. Neuronal activity in the human lateral temporal lobe. II. Responses to the subjects own voice. Exp Brain Res. 77:476–489.
Crone NE, Boatman D, Gordon B, Hao L. 2001. Induced electrocorticographic gamma activity during auditory perception. Clin Neurophysiol. 112:565–582.
Damasio H, Frank R. 1992. Three-dimensional in vivo mapping of brain lesions in humans. Arch Neurol. 49:137–143.
Dejerine J. 1895. Anatomie des centres nerveux. Paris: Rueff et Cie.
Edwards E, Soltani M, Deouell LY, Berger MS, Knight RT. 2005. High gamma activity in response to deviant auditory stimuli recorded directly from human cortex. J Neurophysiol. 94:4269–4280.
Edwards E, Soltani M, Kim W, Dalal SS, Nagarajan SS, Berger MS, Knight RT. 2009. Comparison of time–frequency responses and the event-related potential to auditory speech stimuli in human cortex. J Neurophysiol. 102:377–386.
Fecteau S, Armony JL, Joanette Y, Belin P. 2005. Sensitivity to voice in human prefrontal cortex. J Neurophysiol. 94:2251–2254.
Focke NK, Yogarajah M, Bonelli SB, Bartlett PA, Symms MR, Duncan JS. 2008. Voxel-based diffusion tensor imaging in patients with mesial temporal lobe epilepsy and hippocampal sclerosis. Neuroimage. 40:728–737.
Frank R, Damasio H, Grabowski TJ. 1997. Brainvox: an interactive, multimodal visualization and analysis system for neuroanatomical imaging. Neuroimage. 5:13–30.
Fullerton BC, Pandya DN. 2007. Architectonic analysis of the auditory-related areas of the superior temporal region in human brain. J Comp Neurol. 504:470–498.
Fuster JM. 2008. The frontal cortex. Amsterdam, the Netherlands: Elsevier.
Galaburda AM, Sanides F. 1980. Cytoarchitectonic organization of the human auditory cortex. J Comp Neurol. 190:597–610.
Glasser MF, Rilling JK. 2008. DTI tractography of the human brain's language pathways. Cereb Cortex. 18:2471–2482.
Greenlee JD, Oya H, Kawasaki H, Volkov IO, Kaufman OP, Kovach C, Howard MA, Brugge JF. 2004. A functional connection between inferior frontal gyrus and orofacial motor cortex in human. J Neurophysiol. 92:1153–1164.
Greenlee JD, Oya H, Kawasaki H, Volkov IO, Severson MA, III, Howard MA, III, Brugge JF. 2007. Functional connections within the human inferior frontal gyrus. J Comp Neurol. 503:550–559.
Gross DW, Concha L, Beaulieu C. 2006. Extratemporal white matter abnormalities in mesial temporal lobe epilepsy demonstrated with diffusion tensor imaging. Epilepsia. 47:1360–1363.
Hackett TA. 2008. Anatomical organization of the auditory cortex. J Am Acad Audiol. 19:774–779.
Hackett TA. 2011. Information flow in the auditory cortical network. Hear Res. 271:133–146.
Hackett TA. 2007. Organization and correspondence of the auditory cortex of humans and nonhuman primates. In: Kaas JH, editor. Evolution of the nervous system. Oxford: Elsevier. p. 109–119.
Hackett TA. 2003. The comparative anatomy of the primate auditory cortex. In: Ghazanfar AA, editor. Primate audition: ethology and neurobiology. Boca Raton, FL: CRC Press. p. 199–219.
Hackett TA, Preuss TM, Kaas JH. 2001. Architectonic identification of the core region in auditory cortex of macaques, chimpanzees, and humans. J Comp Neurol. 441:197–222.
Hackett TA, Stepniewska I, Kaas JH. 1999. Prefrontal connections of the parabelt auditory cortex in macaque monkeys. Brain Res. 817:45–58.
Hall DA, Johnsrude IS, Haggard MP, Palmer AR, Akeroyd MA, Summerfield AQ. 2002. Spectral and temporal processing in human auditory cortex. Cereb Cortex. 12:140–149.
Hart HC, Palmer AR, Hall DA. 2004. Different areas of human non-primary auditory cortex are activated by sounds with spatial and nonspatial properties. Hum Brain Mapp. 21:178–190.
Howard MA, Volkov IO, Granner MA, Damasio HM, Ollendieck MC, Bakken HE. 1996. A hybrid clinical-research depth electrode for acute and chronic in vivo microelectrode recording of human brain neurons. Technical note. J Neurosurg. 84:129–132.
Howard MA, Volkov IO, Mirsky R, Garell PC, Noh MD, Granner M, Damasio H, Steinschneider M, Reale RA, Hind JE *et al*. 2000. Auditory cortex on the posterior superior temporal gyrus of human cerebral cortex. J Comp Neurol. 416:76–92.
Kaas JH, Hackett TA. 2005. Subdivisions and connections of auditory cortex in primates: a working model. In: Konig R, Heil P, Budinger E, Scheich H, editors. Auditory cortex: a synthesis of human and animal research. Mahwah, NJ: Erlbaum.
Kaas JH, Hackett TA. 1999. 'What' and 'where' processing in auditory cortex. Nat Neurosci. 2:1045–1047.
Kelly C, Uddin LQ, Shehzad Z, Margulies DS, Castellanos FX, Milham MP, Petrides M. 2010. Broca's region: linking human brain functional connectivity data and non-human primate tracing anatomy studies. Eur J Neurosci. 32:383–398.
Kier EL, Staib LH, Davis LM, Bronen RA. 2004a. Anatomic dissection tractography: a new method for precise MR localization of white matter tracts. Am J Neuroradiol. 25:670–676.
Kier EL, Staib LH, Davis LM, Bronen RA. 2004b. MR imaging of the temporal stem: anatomic dissection tractography of the uncinate fasciculus, inferior occipitofrontal fasciculus, and Meyer's loop of the optic radiation. Am J Neuroradiol. 25:677–691.
Liegeois-Chauvel C, Musolino A, Chauvel P. 1991. Localization of the primary auditory area in man. Brain. 114:139–151.

Matsumoto R, Nair DR, LaPresto E, Bingaman W, Shibasaki H, Luders HO. 2007. Functional connectivity in human cortical motor system: a cortico-cortical evoked potential study. Brain. 130:181–197.
Matsumoto R, Nair DR, LaPresto E, Najm I, Bingaman W, Shibasaki H, Luders HO. 2004. Functional connectivity in the human language system: a cortico-cortical evoked potential study. Brain. 127:2316–2330.
Moran NF, Lemieux L, Kitchen ND, Fish DR, Shorvon SD. 2001. Extrahippocampal temporal lobe atrophy in temporal lobe epilepsy and mesial temporal sclerosis. Brain. 124:167–175.
Mueller SG, Laxer KD, Cashdollar N, Buckley S, Paul C, Weiner MW. 2006. Voxel-based optimized morphometry (VBM) of gray and white matter in temporal lobe epilepsy (TLE) with and without mesial temporal sclerosis. Epilepsia. 47:900–907.
Nathan SS, Sinha SR, Gordon B, Lesser RP, Thakor NV. 1993. Determination of current density distributions generated by electrical stimulation of the human cerebral cortex. Electroencephalogr Clin Neurophysiol. 86:183–192.
Ojemann GA, Engel J, Jr. 1986. Acute and chronic intracranial recording and stimulation. In: Engel J, Jr, editor. Surgical treatment of epilepsies. New York: Raven Press. p. 263–288.
Oya H, Kawasaki H, Dahdaleh NS, Wemmie JA, Howard MA, III. 2009. Stereotactic atlas-based depth electrode localization in the human amygdala. Stereotact Funct Neurosurg. 87:219–228.
Pandya DN, Yeterian EH. 1996. Comparison of prefrontal architecture and connections. Philos Trans R Soc Lond B Biol Sci. 351:1423–1432.
Parker GJ, Luzzi S, Alexander DC, Wheeler-Kingshott CA, Ciccarelli O, Lambon Ralph MA. 2005. Lateralization of ventral and dorsal auditory-language pathways in the human brain. Neuroimage. 24:656–666.
Petrides M, Pandya DN. 1988. Association fiber pathways to the frontal cortex from the superior temporal region in the rhesus monkey. J Comp Neurol. 273:52–66.
Petrides M, Pandya DN. 2002. Comparative cytoarchitectonic analysis of the human and the macaque ventrolateral prefrontal cortex and corticocortical connection patterns in the monkey. Eur J Neurosci. 16:291–310.
Petrides M, Pandya DN. 2009. Distinct parietal and temporal pathways to the homologues of Broca's area in the monkey. PLoS Biol. 7: e1000170.
Petrides M, Pandya DN. 1999. Dorsolateral prefrontal cortex: comparative cytoarchitectonic analysis in the human and the macaque brain and corticocortical connection patterns. Eur J Neurosci. 11:1011–1036.
Powell HW, Parker GJ, Alexander DC, Symms MR, Boulby PA, Wheeler-Kingshott CA, Barker GJ, Noppeney U, Koepp MJ, Duncan JS. 2006. Hemispheric asymmetries in language-related pathways: a combined functional MRI and tractography study. Neuroimage. 32:388–399.
Powell HW, Richardson MP, Symms MR, Boulby PA, Thompson PJ, Duncan JS, Koepp MJ. 2007. Reorganization of verbal and nonverbal memory in temporal lobe epilepsy due to unilateral hippocampal sclerosis. Epilepsia. 48:1512–1525.
Ranck JB. 1975. Which elements are excited in electrical stimulation of mammalian central nervous system: a review. Brain Res. 98:417–440.
Rauschecker JP. 1998. Cortical processing of complex sounds. Curr Opin Neurol. 8:516–521.
Rauschecker JP. 1997. Processing of complex sounds in the auditory cortex of cat, monkey, and man. Acta Otolaryngol Suppl (Stockh). 532:34–38.
Rauschecker JP, Scott SK. 2009. Maps and streams in the auditory cortex: nonhuman primates illuminate human speech processing. Nat Neurosci. 12:718–724.
Rauschecker JP, Tian B. 2000. Mechanisms and streams from processing what and where in auditory cortex. Proc Natl Acad Sci. 97:11800–11806.
Rauschecker JP, Tian B. 2004. Processing of band-passed noise in the lateral auditory belt cortex of the rhesus monkey. J Neurophysiol. 91:2578–2589.
Rauschecker JP, Tian B, Hauser M. 1995. Processing of complex sounds in the macaque nonprimary auditory cortex. Science. 268:111–114.
Reale RA, Calvert GA, Thesen T, Jenison RL, Kawasaki H, Oya H, Howard MA, Brugge JF. 2007. Auditory-visual processing represented in the human superior temporal gyrus. Neuroscience. 145:162–184.
Recanzone GH. 2000. Spatial processing in the auditory cortex of the macaque monkey. Proc Natl Acad Sci USA. 97:11829–11835.
Reddy CG, Dahdaleh NS, Albert G, Chen F, Hansen D, Nourski K, Kawasaki H, Oya H, Howard MA, III. 2010. A method for placing Heschl gyrus depth electrodes. J Neurosurg. 112:1301–1307.
Rilling JK, Glasser MF, Preuss TM, Ma X, Zhao T, Hu X, Behrens TE. 2008. The evolution of the arcuate fasciculus revealed with comparative DTI. Nat Neurosci. 11:426–428.
Rivier F, Clarke S. 1997. Cytochrome oxidase, acetylcholinesterase, and NADPH-diaphorase staining in human supratemporal and insular cortex: evidence for multiple auditory areas. Neuroimage. 6:288–304.
Romanski LM. 2004. Domain specificity in the primate prefrontal cortex. Cogn Affect Behav Neurosci. 4:421–429.
Romanski LM, Averbeck BB. 2009. The primate cortical auditory system and neural representation of conspecific vocalizations. Annu Rev Neurosci. 32:315–346.
Romanski LM, Averbeck BB, Diltz M. 2005. Neural representation of vocalizations in the primate ventrolateral prefrontal cortex. J Neurophysiol. 93:734–747.
Romanski LM, Bates JF, Goldman-Rakic PS. 1999a. Auditory belt and parabelt projections to the prefrontal cortex in the rhesus monkey. J Comp Neurol. 403:141–157.
Romanski LM, Goldman-Rakic PS. 2002. An auditory domain in primate prefrontal cortex. Nat Neurosci. 5:15–16.
Romanski LM, Tian B, Fritz J, Mishkin M, Goldman-Rakic PS, Rauschecker JP. 1999b. Dual streams of auditory afferents target multiple domains in the primate prefrontal cortex. Nat Neurosci. 2:1131–1136.
Rosett J. 1933. Intercortical systems of the human cerebrum, mapped by means of new anatomic methods. New York: Columbia University Press.
Russ BE, Orr LE, Cohen YE. 2008. Prefrontal neurons predict choices during an auditory same-different task. Curr Biol. 18:1483–1488.
Scott SK. 2005. Auditory processing—speech, space and auditory objects. Curr Opin Neurobiol. 15:197–201.
Scott SK, Johnsrude IS. 2003. The neuroanatomical and functional organization of speech perception. Trends Neurosci. 26:100–107.
Sherman SM, Guillery RW. 2006. Exploring the thalamus and its role in cortical function. Cambridge, MA: MIT Press.
Steinschneider M, Nourski KV, Kawasaki H, Oya H, Brugge JF, Howard MA, III. 2011. Intracranial study of speech-elicited activity on the human posterolateral superior temporal gyrus. Cereb Cortex. 21:2332–2347.
Stuss DT, Knight RT. 2002. Principles of frontal lobe function. New York: Oxford University Press.
Sweet RA, Dorph-Petersen KA, Lewis DA. 2005. Mapping auditory core, lateral belt, and parabelt cortices in the human superior temporal gyrus. J Comp Neurol. 491:270–289.
Thivard L, Lehericy S, Krainik A, Adam C, Dormont D, Chiras J, Baulac M, Dupont S. 2005. Diffusion tensor imaging in medial temporal lobe epilepsy with hippocampal sclerosis. Neuroimage. 28:682–690.
Tian B, Reser D, Durham A, Kustov A, Rauschecker JP. 2001. Functional specialization in rhesus monkey auditory cortex. Science. 292:290–293.
Toga AW, Mazziotta JC. 2000. Brain mapping: the systems. San Diego, CA: Academic Press.
Uppenkamp S, Johnsrude IS, Norris D, Marslen-Wilson W, Patterson RD. 2006. Locating the initial stages of speech-sound processing in human temporal cortex. Neuroimage. 31:1284–1296.
Vaadia E. 1989. Single-unit activity related to active localization of acoustic and visual stimuli in the frontal cortex of the rhesus monkey. Brain Behav Evol. 33:127–131.

Vaadia E, Benson DA, Hienz RD, Goldstein MH, Jr. 1986. Unit study of monkey frontal cortex: active localization of auditory and of visual stimuli. J Neurophysiol. 56:934–952.
Voisin J, Bidet-Caulet A, Bertrand O, Fonlupt P. 2006. Listening in silence activates auditory areas: a functional magnetic resonance imaging study. J Neurosci. 26:273–278.
von Economo C. 1929. The cytoarchitectonics of the human cerebral cortex. London: Oxford University Press.
Wallace MN, Johnston PW, Palmer AR. 2002. Histochemical identification of cortical areas in the auditory region of the human brain. Exp Brain Res. 143:499–508.
Walter WG. 1964. The convergence and interaction of visual, auditory, and tactile responses in human nonspecific cortex. Ann NY Acad Sci. 112:320–361.
Waxman SG, Swadlow HA. 1977. The conduction properties of axons in central white matter. Prog Neurobiol. 8:297–324.
Wilson CL, Isokawa M, Babb TL, Crandall PH. 1990. Functional connections in the human temporal lobe. I. Analysis of limbic system pathways using neuronal responses evoked by electrical stimulation. Exp Brain Res. 82:279–292.
Yeomans JS. 1990. Principles of brain stimulation. Oxford: Oxford University Press.